

From nano- to global scales: properties, processes of formation, and aftereffects of atmospheric aerosol impacts.

5. Aerosol and chemical processes in the atmosphere

K.Ya. Kondratyev

*Scientific Research Center for Ecological Safety,
Russian Academy of Sciences, St. Petersburg
Nansen International Environment and Remote Sensing Centre, St. Petersburg*

Received July 7, 2004

The aerosol impacts on the chemical and photochemical processes in the atmosphere are reviewed.

Introduction

The aerosol particles play an important role in heterogeneous chemical reactions with various atmospheric trace gases (TGs) as a climate-forming factor. In addition, the aerosol significantly influences the photochemical processes in the atmosphere. In this connection, it is of primary importance to obtain simultaneously reliable information about the concentration and properties of both the aerosol and TGs.

Fires in savanna form one of the most important factors of ecodynamics in the regions of Southern Africa, whose effect on the atmospheric chemical processes and biogeochemical cycles can show itself not only on regional, but also on the global scales. Such fires occur mostly during dry season (May–October) and are characterized by the presence of significant annual variations in the location and intensity. It is assumed that fires in savannas do not give rise to changes in the CO₂ exchange between the grass cover and the atmosphere, because CO₂ emissions are almost compensated for by the CO₂ consumption in the process of vegetation growth. However, emissions of other trace gases and aerosol are an important consequence of the fires.

One of the most significant characteristics of pyrogenic emissions into the atmosphere is the emission factor (EF) for various trace gases and aerosol particulates, which is the mass of emission of the corresponding component calculated per unit dry mass of the fuel consumed (g/kg). To determine EF, Korontzi et al.¹⁵ initiated artificial grassland and forest fires in the period of June 5–August 6 of 1996 at 13 sites (with the area of 2 hectares), situated 7.5 km southeast of Kaoma (Zambia: 14°52' S, 24°49' E; 1170 m above the sea level). In Ref. 15, the authors present the first early dry season (early June–early August) emission factor measurements for carbon dioxide (CO₂), carbon monoxide (CO), methane (CH₄), nonmethane hydrocarbons (NMHC), and particulates with a diameter less than 2.5 μm (PM_{2.5}). It was found that seasonal emission factors

for grassland fires correlate linearly with the proportion of green grass, used as a surrogate for the fuel moisture content, and are higher for products of incomplete combustion in the early part of the dry season compared with that later in the dry season. Models of emission factors for NMHC and PM_{2.5} versus modified combustion efficiency (MCE) are statistically different in grassland compared with woodland ecosystems.

Korontzi with co-workers¹⁵ compared predictions based on the integration of emissions factors from this study, from the Southern African Fire-Atmosphere Research Initiative 1992 (SAFARI-92), and from SAFARI-2000 with those based on the smaller set of ecosystem-specific emission factors to estimate the effects of using regional-average rather than ecosystem-specific emission factors. They also tested the validity of using the SAFARI-92 models for emission factors versus MCE to predict the early dry season emission factors measured in that study. The comparison has indicated that the largest discrepancies occur at the low end (0.907) and high end (0.972) of MCE values measured in this study. Finally, Korontzi et al. combined their models of MCE versus proportion of green grass for grassland fires with emission factors versus MCE for selected oxygenated volatile organic compounds measured in the SAFARI-2000 campaign to derive the first seasonal emission factors for these compounds. The results of that study have demonstrated that seasonal variations in savanna fire emissions are important and should be considered in modeling emissions at regional to continental scales.

Continental China has been recognized as one of the most important sources of atmospheric mineral dust particles (called Kosa in Japan, which literally means yellow sand). Many investigators have pointed out the importance of study of the long-range transport of mineral dust particles and their modifications in this process even in the absence the dust storms. Because of these modifications, particles can change their radiative properties and their ability to be condensation nuclei. Trochkin et al.²⁷ have

analyzed aerosol samples collected in Dunhuang, North-Western China, in different seasons in 2001 and 2002 during the ACE-Asia campaign. The collected particles, mostly of mineral origin, were examined using a scanning electron microscope equipped with an energy dispersive X-ray analyzer.

About 46–77% of particles had an increased content of Si (mostly due to quartz and aluminum silicates), while 13 to 41% of particles had an increased content of Ca (mostly in the form of calcite CaCO_3 , dolomite $\text{CaMg}(\text{CO}_3)_2$, and mineral white $\text{CaSO}_4 \times 2\text{H}_2\text{O}$). Particles enriched with iron (nitrogen oxides) made up a marked part (3 to 10%). Similar types of mineral particles were also observed in the free troposphere over Japan, but a number of differences were found between the particles collected in China and those collected over Japan, and these differences can be explained by chemical modifications that occurred in the particles during their transport from China to Japan. Approximately 40 to 45% of mineral particles mixed internally with sulfate during their transport in the troposphere. Also, the particles collected over Japan were found to be different from those obtained in ground-based measurements in Nagasaki, Nagoya, and Fukuoka, Japan (reported by other research groups). The portion of mineral particles that mixed internally with the sea salt and sulfates was considerably smaller than in the samples obtained in Japan near the ground. It is important to take this fact into account while investigating the impact of mineral particles on the biogeochemical cycle and climate.

In order to evaluate the impact of Asian dust on the air quality of North America, Liu with co-workers²⁰ applied a relatively new type of factor analysis, positive matrix factorization (PMF), to the $\text{PM}_{2.5}$ particle composition data obtained at two, high elevated, sampling sites in the western United States from Interagency Monitoring of Protected Visual Environments (IMPROVE) program. These two sites were Crater Lake National Park (42.89° N, 122.14° W, 1981 m above the sea level) and Lassen Volcanic National Park (40.54° N, 121.58° W, 1798 m). The PMF can provide optimal point-by-point weighting by using the estimates uncertainty in the data and can permit efficient treatment of missing and below detection limit values. The factors were normalized using fine aerosol mass concentration data through multiple linear regression so that the quantitative source contributions for each resolved factor were obtained.

Among the six and seven sources resolved at the two sites, six were common. These six sources exhibited not only similar chemical compositions but also similar seasonal variations at both sites. The Asian dust was represented by Al, Ca, Fe, NO_3 , S, K, and Ti with strong seasonal variation. Secondary sulfate with a high concentration of S and strong seasonal variation correlated with the Asian dust. Wood smoke was represented by organic carbon (OC), elemental carbon (EC), and K; sea salt with

the high concentrations of Na, S, and NO_3 have been taken into account. Nitrate was dominated by NO_3 and motor vehicle exhausts with high concentrations of OC, EC, and dust elements. An incinerator source with the presence of Cu and Zn also was resolved from the Crater Lake site. Generally, most of the sources at these two sites showed similar chemical composition profiles and seasonal variation patterns. This study indicated that PMF was a powerful factor analysis method to isolate sources from the ambient aerosol concentration data.

During the 2001 Aerosol Characterization Experiment (ACE)-Asia and the Transport and Chemical Evolution over the Pacific (TRACE-P) experiments, Lee with co-workers¹⁸ measured, respectively, eight inorganic ions in fine aerosol particles on board the NCAR C130 and NASA P-3B aircraft. Concentrations of NH_4^+ , SO_4^{2-} , NO_3^- , Ca^{2+} , K^+ , Mg^{2+} , Na^+ , and Cl^- were determined using a particle-into-liquid sampler coupled to ion chromatography (PILS-IC) technique at a 4-min resolution and a limit of detection $< 0.05 \mu\text{g}/\text{m}^3$. The maximum total ion concentrations observed on the C130 and the P-3B were $27 \mu\text{g}/\text{m}^3$ and $84 \mu\text{g}/\text{m}^3$, respectively.

During ACE-Asia, NH_4^+ and SO_4^{2-} dominated, with the dust-derived Ca^{2+} contributing nearly equally with SO_4^{2-} in the mixing ratios. The sea-salt-derived Na^+ and Cl^- were comparable to biomass-burning tracer K^+ . During TRACE-P, NH_4^+ dominated, followed by SO_4^{2-} , Cl^- , Na^+ , NO_3^- , Ca^{2+} , and K^+ , in decreasing order of importance. In addition to the sea-salt origin, Cl^- showed a source in urban emissions possibly related to biofuel combustion. Both sea salt and dust contributed to Mg^{2+} content.

In both experiments, NH_4^+ , SO_4^{2-} , NO_3^- , and CO strongly correlated, indicating that combustion was the dominant source of these species and that NH_3 and other alkaline materials were sufficient to neutralize H_2SO_4 . The $[\text{NH}_4^+]$ to $([\text{NO}_3^-] + 2[\text{SO}_4^{2-}])$ ratio was ~ 0.70 in the two campaigns, with deviations found only in volcanic plumes, whereby SO_4^{2-} was found to correlate with SO_2 . Charge balance of the ions showed both positive and negative deviations whose magnitudes, $\sim 30\%$, provide estimates of the lower limits of unmeasured ions. Elevated NO_3^- and Ca^{2+} coexist mainly under polluted conditions, suggesting the importance of sequestering HNO_3 by mineral dust.

Low molecular weight dicarboxylic acids, such as oxalic, malonic, and succinic, were found in the atmospheric aerosol both in the continental and maritime atmosphere. Tropospheric aerosols were collected during C130 aircraft campaign over the east Asia/Pacific region in April to May 2001 and were analyzed for low molecular weight dicarboxylic acids.¹⁴ Homologous series of $\text{C}_2\text{--C}_3$ dicarboxylic

acids were detected, for the first time, in the polluted troposphere in the Asian region using aircraft. Oxalic acid (C_2) was found to be the most abundant species followed by malonic (C_3) or succinic (C_4) acid. Total concentrations of C_2 – C_5 diacids (44 – 870 ng/m^3 , average 310 ng/m^3) were similar to those reported in urban area of Tokyo near the ground level.

Concentrations of oxalic acid showed a positive correlation ($r^2 = 0.70$) with total organic carbon (TOC), although other diacids showed weaker positive correlation. These results suggest that water-soluble dicarboxylic acids and TOC were emitted from similar sources on the ground in the Asian continent and/or produced by the photochemical oxidation of anthropogenic organic compounds in the atmosphere. The diacid-carbons were found to comprise 0.2 – 3.3% (average 1.8%) of TOC. Water-soluble dicarboxylic acids may play an important role in controlling the chemical and physical properties of organic aerosols in the polluted troposphere over eastern Asia and the western Pacific.

Differences in the chemical composition between the sea-salt aerosol (SSA) and seawater were widely discussed earlier. One of the characteristic features of these differences is the decreased chloride content relative to sodium in SSA as compared to seawater. At the chloride deficit in air over the sea surface in the range of 5 – 30 $nmol/m^3$, the estimated concentration of HCl was 110 – 670 ppb (that is, 200 – 1100 ng/m^3). However, the chloride deficit was estimated from the data on the $[Cl^-]/[Na^+]$ concentration ratio in aerosol samples on filters, relative to which it is possible to assume the presence of the acid-induced remobilization of chlorine, which distorts the aerosol composition.

The analysis of impactor aerosol samples with allowance for the particle size differentiation, carried out by Jourdain and Legrand¹² in January 1998 at the coastal Antarctic observation site, revealed the mean chloride loss of $\sim 70\%$, but the data on HCl were still lacking for these conditions. In this connection, the year-round composition of bulk and size-segregated aerosol was examined at a coastal Antarctic site (Dumont d'Urville; $60^\circ 40' S$, $140^\circ 01' E$) starting from 1991. Sea-salt particles displayed a summer depletion of chloride relative to sodium, which reached $\sim 10\%$. The mass chloride loss was maximum on 1 - to 3 - μm -diameter particles, nitrate being often the anion causing the chloride loss. The summer $[SO_4^{2-}]/[Na^+]$ ratio exceeded the seawater value on submicron particles due to biogenic sulfate and on coarse particles due to ornithogenic (guano-enriched soils) sulfate and to heterogeneous uptake of SO_2 (or H_2SO_4). HCl levels ranged from (41 ± 28) ng/m^3 in winter to (130 ± 110) ng/m^3 in summer, being close to the mass chloride loss of sea-salt aerosols. In winter, sea-salt particles exhibit $[Cl^-]/[Na^+]$ and $[SO_4^{2-}]/[Na^+]$ mass ratios of 1.9 ± 0.1 and 0.13 ± 0.04 , respectively.

Resulting from precipitation of mirabilite during freezing of seawater, this sulfate-depletion relative

sodium takes place from May to October. From March to April, warmer temperatures and/or smaller sea ice extent offshore the observation site limits the phenomenon. A range of 14 – 50 ng/m^3 of submicron sulfate was found, confirming the existence of nss- SO_4^{2-} in winter at a coastal Antarctic site, highest values being found in winters of 1992–1994 due to the Pinatubo volcanic eruption. Apart from these three winters, the nss- SO_4^{2-} levels range between 15 and 30 ng/m^3 , but its origin is still unclear (quasi-continuous SO_2 emissions from the Mount Erebus volcano or local wintertime dimethyl sulfide [DMS] oxidation, in addition to long-range transport by-product of the DMS oxidation).

The examples considered illustrate the complexity and variety of the chemical composition of both aerosol and atmospheric trace gases. Now let us discuss the observations and capabilities of numerical simulation of the interaction between aerosol and trace gases.

1. Interaction between aerosol and trace gases

Factors controlling the content of ozone and aerosol in the atmosphere are atmospheric emissions of these constituents and their precursors, as well as chemical reactions and meteorological processes. All these factors depend interactively on varying climate conditions. In this connection, Liao with co-workers^{19a} developed a unified tropospheric chemistry–aerosol model within the Goddard Institute for Space Studies general circulation model (GISS GCM II). The model includes a detailed simulation of tropospheric ozone– NO_x –hydrocarbon chemistry as well as aerosols and aerosol precursors. Predicted aerosol species include sulfate, nitrate, ammonium, black carbon, primary organic carbon, and secondary organic carbon. The model takes into account the influence of all types of aerosol on the photolysis rates; heterogeneous reactions with the participation of N_2O_5 , NO_3 , NO_2 , and HO_2 on moistened surfaces of aerosol particles, and the uptake of SO_2 , HNO_3 , and O_3 by mineral dust particles.

Although the current version of the unified model does not include a prognostic treatment of mineral dust (MD), its effects on photolysis and heterogeneous processes are taken into account by using three-dimensional off-line fields determining the MD concentration. The partitioning of ammonia and nitrate between gas and aerosol phases is determined by on-line thermodynamic equilibrium, and the formation of secondary organic aerosols is based on equilibrium partitioning and experimentally determined parameters. Two-way coupling between aerosols and chemistry provides consistent chemical fields for aerosol dynamics and aerosol mass for heterogeneous processes and calculations of the gas-phase photolysis rates. Considering both mineral dust

uptake of HNO_3 and wet scavenging of HNO_3 on ice leads to a closer agreement between the predicted gas-phase HNO_3 concentrations and measurements than in previous global chemical transport model simulations, especially in the middle to upper troposphere.

As a result of the coupling between chemistry and aerosols, global burdens of both gas-phase and aerosol species are predicted to respond nonlinearly to changing emissions of NO_x , NH_3 , and sulfur. The unified model has allowed the simulation to be done of sulfate and nitrate aerosols that are associated with mineral dust. Near regions being sources of dust, more than 50% of total sulfate near the surface are formed just in this way. On the global scale, the formation of nitrate aerosol on dust particles exceeds the scales of formation of this aerosol due to ammonium nitrate.

The numerical simulation discussed has shown that the influence of aerosol (on the global scale) on the chemical processes with the participation of trace gases caused by the changes in the photolysis rate is low. However, heterogeneous processes are important for both trace gases and aerosol. Although the total surface area of MD particles makes up only a small fraction of the total surface area of all global aerosol particles, the particles of mineral aerosol play an important role in uptake of such trace gases as O_3 , SO_2 , and NH_3 . However, the contribution of heterogeneous reactions on the surface of aerosol particles (especially, MD aerosol) is still estimated very roughly. The interaction between aerosol and chemical processes with the participation of trace gases is also of great importance, because the formation of sulfates in clouds depends on changes in the O_3 concentration and/or on changes in pH of cloud droplets during the aerosol formation. On the other hand, the formation of sulfate or nitrate aerosol associated with MD particles depends on alkalinity of MD particles and on the presence of gaseous HNO_3 and SO_2 . Such interactive processes lead to the nonlinear dependence of the content of trace gases and aerosol on emissions of sulfate compounds and ammonium.

Jacobson¹⁰ proposed new and modified numerical techniques for solving the size- and time-dependent aerosol processes of nucleation, coagulation, condensation, dissolution, and reversible chemistry among multiple aerosol particle size distributions and the gas phase and over the entire relative humidity (RH) range. The techniques treat particle number, mole, and volume concentrations, solution and nonsolution densities, and refractive index consistently. Some findings included the following:

(1) Coagulation internally mixes particles of different original composition over the entire size distribution.

(2) Coagulation internally mixes a greater fraction of larger than smaller particles.

(3) Coagulation internally mixes larger particles with other distributions more than it does with smaller particles.

(4) Coagulation among multiple distributions produces the same summed size distribution as coagulation of a single distribution when the sum of initial distributions is the same in both cases.

(5) In a competition for vapor between homogeneous nucleation and condensation, the relative importance of condensation increases with an increasing number of background particles.

(6) In the absence of a continuous source of new particles, coagulation, condensation, dissolution, hydration, and chemical reaction internally mix most particles within half a day under moderately polluted conditions.

(7) Condensation increases the fractional coating of small particles more than of the large ones.

(8) The real refractive index of a particle containing electrolytes is higher at low RHs than at high RHs.

(9) The difference between total particle and solution real refractive indices increases with decreasing RH.

(10) Real part of the refractive index of a solution generally increases with the decreasing particle size.

The earlier numerical simulation of the processes of formation and transformation of the global dust aerosol has allowed the approximate reconstruction of the dust aerosol transport and the following deposition onto the surface under current climatic conditions. However, none of the existing models succeeded in reliable reconstruction of the emission rate of sources of dust aerosol in Sahara and Asia. All models overestimated the emissions of dust aerosol and its transport from Australia.

An important circumstance is that dust emissions from the surface into the atmosphere are strongly controlled by the properties of the vegetation cover. Thus, for example, under conditions of semiarid climate, the fast growth of the grass cover (after precipitation) suppress dust emissions for the period from some days to few weeks, whereas the presence of bushes causes a significant decrease of emissions even in the period when there are no leaves. Even in regions with poor vegetation, the surface not everywhere is an intense source of dust. The concentration of dust aerosol emissions is observed in the regions, where recent geomorphological evolution gave rise to the concentration of fine-grain material and led to formation of vast surface areas having low roughness (this applies, for example, to surfaces of the bed of dry paleolakes).

In this connection, Tegen with co-workers²⁶ proposed a new model of the dust cycle that successfully predicts dust emissions as determined by land surface properties, monthly vegetation and snow cover, and 6-hour surface wind speeds for the years 1982–1993. The model takes account of the role of dry lakebeds as a preferential source area for dust emission. The dust source scheme also explicitly takes into account the role of vegetation type as well as monthly vegetation cover. Dust transport was

computed using assimilated winds for the years 1987–1990. Deposition of dust occurs through dry and wet deposition, where subcloud scavenging is calculated using assimilated precipitation fields. Comparison of simulated patterns of atmospheric dust loading with the Total Ozone Mapping Spectrometer satellite absorbing aerosol index shows that the model yields quite realistic results from daily to interannual timescales.

The amount of deposited dust agrees well with the sediment flux data from marine sites. Emissions of submicron dust from preferential source areas are required for computation of a realistic dust optical thickness. Sensitivity studies have shown that Asian dust source strengths are particularly sensitive to the seasonality of vegetation cover. The global level of dust emissions was estimated as 800 Mt/year, but with the allowance for intensification of dust emissions in the regions of Sahara, China, Australia, and Arabia, this value increases up to 1700 Mt/year. Therefore, the global emissions should be estimated as ranging from 800 to 1700 Mt/year (instead of the earlier extreme values equal to 60 and 3000 Mt/year).

Bian and Zender³ investigated the influence of mineral dust on tropospheric chemistry in the present climate on the global scale. The analysis examined the effects of dust on photolysis and heterogeneous uptake, operating independently and together. In numerical experiments, the size-resolved, time-varying mineral dust distribution predicted by the global Dust Entrainment and Deposition (DEAD) model perturbed the gas phase species in a global chemical transport model (University of California at Irvine (UCI) CTM). The Table presents the results calculated at a separate consideration of only photolysis or heterogeneous processes, as well as at the joint consideration of both factors (NATA is an abbreviation for the regions of north Africa and tropical Atlantic Ocean) for the northern (NH) and southern hemispheres (SH), and for the whole globe. The coupling coefficient k , characterizing the nonlinear coupling between photolysis and heterogeneous reactions, is determined by the equation

$$k = \Delta_{p+H} / (\Delta_p + \Delta_H).$$

If k is close to unity, this means that the contributions Δ_p and Δ_H are additive (that is,

nonlinearity does not show itself). As can be seen from the Table, for the most trace gases under consideration the changes in concentration do not exceed several percent, except for hydroxyl OH (–11.1%).

As would be expected, the widest changes are observed in the regions situated downwind from the dust source regions (north Africa, tropical Atlantic Ocean, Arabia). Dust-induced changes in the concentration of O₃ and OH in the Northern Hemisphere more than 5 times exceed those observed in the Southern Hemisphere. The regional features are characterized by the fact that the photolysis perturbation dominates in limited regions from the low to middle troposphere, while heterogeneous uptake dominates in the rest part of the atmosphere. Coupling of the photochemical and heterogeneous effects of dust is weak in the global mean but moderate in dusty regions, where coupling is sometimes responsible for more than 20% of local O₃ changes.

Ozone and odd nitrogen concentrations are perturbed in opposite directions by photolysis and heterogeneous chemistry, resulting in a weak net change. However, both processes decrease the concentrations of OH and HO₂. The global mean change due to dust is –0.7% for tropospheric O₃, –11.1% for OH, –5.2% for HO₂, and –3.5% for HNO₃. Large seasonal signals are present near dust source regions. Over the North African region and tropical Atlantic Ocean downwind, OH decreases by –66.8%, six times higher than the global mean reduction.

Interestingly, net photolysis-induced annual mean O₃ changes are greater in the Southern Hemisphere than in the Northern Hemisphere, where significantly more dust and O₃ precursors reside. In polar regions, O₃ change is dominated by transported O₃ and is not sensitive to local dust concentration. O₃ change due to photolysis depends not only on dust vertical structure but also on the presence of O₃ precursors. O₃ change due to heterogeneous reactions on dust is sensitive to dust vertical structure, mainly through the influence of temperature on uptake rates. Bian, Prather, and Takemura² emphasized that these results are tentative and it is necessary to obtain quite complete observations (needed to check the adequacy of the numerical simulation).

Table. Annual mean changes (%) in the concentration of eight trace gases due to dust

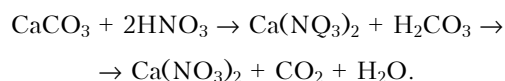
Trace gas	Photolysis, Δ_p				Heterogeneous reactions, Δ_H				Coupling, Δ_{p+H}					k
	NH	SH	Globe	NATA	NH	SH	Globe	NATA	NH	SH	Globe	NATA	Globe	
O ₃	0.2	0.3	0.2	0.9	–1.5	–0.3	–0.9	–5.0	–1.3	–0.0	–0.7	–3.8	1.00	0.93
OH	–4.0	–0.8	–2.4	–15.0	–16.4	–2.9	–9.6	–64.0	–18.5	–3.6	–11.1	–66.8	0.93	0.85
HNO ₃	0.4	0.3	0.3	0.8	–6.1	–1.5	–3.8	–28.3	–5.8	–1.2	–3.5	–27.7	1.00	1.01
HO ₂	–1.0	0.2	–0.4	–6.0	–9.1	–1.1	–5.1	–43M5	–9.6	–0.9	–5.2	–45.3	0.95	0.92
NO ₃	1.9	0.8	1.3	5.4	–10.2	–1.5	–5.9	–47.2	–8.7	–0.8	–4.7	–44.2	1.02	1.06
NO ₂	2.1	0.7	1.4	9.8	–0.5	–0.2	–0.3	–6.9	1.6	0.5	1.1	3.1	1.00	1.07
N ₂ O ₅	3.3	1.2	2.2	12.0	–3.4	–0.8	–2.1	–19.6	–0.3	0.4	0.0	–9.4	–	1.24
H ₂ O ₂	0.3	0.7	0.5	–0.6	–0.4	0.1	–0.2	–2.2	–0.2	0.8	0.3	–3.0	1.00	1.07

In the context of parameterization of the interaction between aerosol and trace gases, Hynes with co-workers⁹ have carried out the laboratory investigations of the uptake of HNO₃ on water-ice films in a coated wall flow reactor under tropospheric temperature conditions (210–235 K). Experiments were performed in the “ice” region of the HNO₃–H₂O phase diagram. With HNO₃ partial pressures in the range of (0.3–2.0) · 10^{–6} Torr, continuous uptake was observed below 215 K; whereas above 215 K, the uptake was time dependent. By assuming that the surface coverage can be represented by a Langmuir isotherm for the dissociative adsorption, the enthalpy of adsorption of HNO₃ onto ice was found to be $-(54.0 \pm 2.6)$ kJ/mol.

At a constant HNO₃ partial pressure, the maximum uptake coefficients, γ , were measured as a function of temperature, decreasing from 0.03 at 215 K down to 0.006 at 235 K. The uptake coefficients at 218 K were not significantly affected by changes in HNO₃ partial pressure. The uptake of HCl at 218 K on ice surfaces previously dosed with HNO₃ was found to be reversible, and the coadsorption of HNO₃ with HCl indicates that HCl is displaced from surface sites by HNO₃ molecules. Uptake of HNO₃ on HCl-dosed surfaces showed that HNO₃ molecules displace $\sim 10^{13}$ molecules/cm³ of HCl. In this context, the efficiency of cirrus clouds in scavenging HNO₃ was discussed, as well as the implications for chloride activation reactions under tropospheric temperature conditions.

Every year 1000 to 3000 Tg (terragram) of mineral (dust) aerosol lifted by wind from the surface come into the atmosphere. According to the available estimates, the currently active expansion of arid regions will lead to the increase in the atmospheric content of dust aerosol. Since fine mineral aerosol particles have a relatively long lifetime in the atmosphere, they are subject to the long-range transport, during which they can take part in heterogeneous chemical reactions with various atmospheric trace gases. Such reactions may result in the change of the gas-phase chemical budget, as well as chemical properties of the aerosol particles. The changes in such physical characteristics of aerosol as the particle size and shape, chemical composition, and hygroscopic property, in their turn, affect the optical properties of aerosol and, as a consequence, the character of aerosol impact on climate.

Chemically active calcium carbonate is an abundant component of the dust aerosol. Since nitric acid vapor is one of the atmospheric trace gases, the following reactions are possible:



The available data indicate that the chemical activity of HNO₃ intensifies considerably in the presence of water vapor, and solid particles of calcium carbonate transform into droplets of the aqueous solution of calcium nitrate in the course of

the above reaction, because solid calcium nitrate Ca(NO₃)₂ (s) transforms into liquid Ca(NO₃)₂ (aq). The transformation of solid particles into liquid droplets through heterogeneous chemical reactions is very important in the context of the aerosol impact on climate. Using Scanning Electron Microscopy (SEM) and Energy Dispersive X-Ray (EDX) laboratory analysis, Krueger with co-workers¹⁶ showed that individual calcium carbonate particles reacted with gas-phase nitric acid at 293 K. The SEM images clearly showed that solid CaCO₃ particles are converted into spherical droplets as the reaction proceeds. The process occurs through a two-step mechanism involving the conversion of calcium carbonate into calcium nitrate followed by the deliquescence of the calcium nitrate product. The change in phase of the particles and the significant reactivity of nitric acid and CaCO₃ at low RH are a direct result of the deliquescence of the product at low RH.

The atmospheric photolysis of nitrous acid (HONO) is one of the important sources of OH radicals in the polluted atmosphere. It has been found that HONO is formed through the transformation of nitrogen oxides NO_x on the surface of atmospheric aerosol particles, but the mechanism of this transformation is currently not well understood. To study the mechanism of this heterogeneous conversion, Wang with co-workers²⁸ carried out the measurements of HONO and NO₂ in Phoenix (USA) in summer 2001 using long path (about 3.3 km) DOAS (differential optical absorption spectroscopy). These measurements showed that ratios of chemically formed secondary [HONO] to [NO₂] rarely exceeded 3%. During two nocturnal dust storm events, however, a significant increase of this ratio was observed. The unprecedented high ratios near 19% suggest a highly efficient NO₂ to HONO conversion process on mineral dust particles. The particle composition in Phoenix is similar to other mineral dusts, implying that the enhanced NO₂ conversion could be an important HONO, and therefore also OH, source in regions where pollution and dust storms coincide.

Jordan et al.¹¹ discussed the results of analysis of aerosol data collected near Asia on the DC-8 aircraft platform during TRACE-P. These data have been examined for evidence of the uptake of NO₃[–] and SO₄^{2–} on particle surfaces of dust aerosol, coming mostly from Chinese deserts, by comparing the data corresponding to the dusted and clear atmosphere. The dusted air was also characterized by increased concentration of such anthropogenic trace gases as HNO₃, SO₂, and CO, which was higher in the dust sector than in the clean sector by factors of 2.7, 6.2, and 1.5, respectively. The collocation of dust and pollution sources allowed for the uptake of NO₃[–] and nss-SO₄^{2–} on the coarse dust aerosols, increasing the mixing ratios of these particulates by factors of 5.7 and 2.6 on the average.

There was sufficient $\text{non-sea-salt-SO}_4^{2-}$ to take up all of the NH_4^+ present, with enough excess of $\text{non-sea-salt-SO}_4^{2-}$ to also react with dust CaCO_3 . This suggests that the enhanced NO_3^- was not in fine mode of NH_4NO_3 . Particulate NO_3^- (p- NO_3^-) constituted 54% of the total NO_3^- (t- NO_3^-) on the average, reaching a maximum of 72% in the dust sector. In the dust free sector, p- NO_3^- contributed 37% to t- NO_3^- , likely due to the abundance of sea salts there. In two other sectors where the influence of dust and sea salt were minimum, p- NO_3^- accounted for <15% of t- NO_3^- .

The results obtained in Ref. 11 are indicative of the possibility of significant *in situ* uptake of acid gases on alkaline particles of the dust aerosol, leading to the removal of nitrogen from the atmosphere, which can be of great importance on regional scales. The presence of NO_3^- and SO_4^{2-} ions on the coarse aerosol particles can lead to intensification of acid precipitations and, as a consequence, to the adverse effects on land ecosystems. For marine ecosystems, the intensified deposition of NO_3^- can lead to the deficit of this biogen for the offshore biota. It is natural that such effects can become even more significant under the conditions of further industrialization of the Eastern Asia.

Using a box model, Meier and Hendricks²⁴ numerically simulated potential chemical perturbations in the midlatitude upper troposphere caused by the reactive and nonreactive uptake of trace gases on cirrus ice particles. Chemical implications of denoxification caused by heterogeneous reactions with HNO_3 as a product and adsorption of gas phase HNO_3 on ice surfaces were the special focus.

The simulations suggested that cirrus cloud chemistry has the potential to induce strong local reductions in the upper tropospheric HNO_3 and NO_x . Because of NO reduction, the OH/ HO_2 ratio and the OH concentration decrease. As a consequence of these effects, a significant reduction in the net ozone production rate was modeled. Sensitivity studies were performed varying the HNO_3 adsorption efficiency, the particle sedimentation efficiency, and the ambient NO_x concentration.

The sensitivity experiments revealed that the modeled cirrus cloud impacts are mainly driven by the nonreactive uptake of HNO_3 on ice particles and the subsequent particle sedimentation. The effects strongly depend on the efficiency of HNO_3 adsorption. If a very efficient uptake of HNO_3 is assumed, decreases in the ozone mixing ratio down to 14% were modeled. The simulations also suggested that the cirrus cloud impact on ozone is sensitive to the ambient NO_x concentration. Chloride activation due to heterogeneous reactions on cirrus ice particles has a minor effect on the model ozone chemistry under the conditions regarded. The model calculations further suggested that chemical

perturbations caused by the uptake of OH, HO_2 , and H_2O_2 on ice are potentially significant only in periods of high cirrus cloud activity. Observational data on cirrus chemical impacts in the upper troposphere are currently too sparse to perform a detailed model validation.

It is commonly recognized now that under the conditions of formation of intense smog the main part of aerosol organic carbon is formed due to secondary processes of gas-phase transformation with biogenic precursors being important contributors. Since nucleation processes are determined by contributions from several components, there is no need (for formation of particles) in the high level of supersaturation with respect to some individual component. In particular, this means that the formation of particles can proceed at a relatively low concentration of biogenic aerosol precursors. Even if the conditions appear to be unfavorable for homogeneous nucleation, the processes of formation of ultrafine particles can occur due to the mechanisms of ionic nucleation. Organic aerosol formed in this way can undergo further transformation as a result of reactions with participation of free radicals and hydroxyl radical.

Although the humus matter makes up about 70% of all organic matter in global continental and water pools, the relation between these giant pools and the composition of fine organic aerosol is still unclear. In this connection, Gelencsér with co-workers⁶ presented a novel hypothesis for a possible formation mechanism of humic-like substances, which were shown to be ubiquitous in fine continental aerosol. It tentatively relates the formation of atmospheric humic matter to the vast pool of soil organic matter via the evaporation, condensation, and aerosol-phase polymerization of low molecular weight polar degradation products of organic debris in the soil.

This theory⁶ is based on a comparative study of the chemical structure of bulk organic matter in fine aerosol and natural humic and fulvic acids. Although the total soil flux of all degradation products is estimated to be of the order of $1 \text{ ng} \cdot \text{m}^{-2} \cdot \text{s}^{-1}$, which is very low and difficult to measure, it is sufficient to sustain a mass concentration comparable to that of fine organic aerosol. The results imply that the proposed formation mechanism may be a significant natural source for fine organic aerosol at continental sites. It is also supposed that precursors from other anthropogenic and natural sources contribute to producing secondary humic-like polymeric matter in continental fine aerosol. This hypothesis certainly calls for confirmation with the experimental data.

The distribution of nitrate among the gas and aerosol phases significantly influences the chemical reactions in the troposphere and the formation of biogeochemical cycles of nitrogen compounds. In particular, it is important that nitric acid (HNO_3) vapor can react with ammonia (NH_3), leading to formation of fine ammonium nitrate aerosol. The content of gaseous nitric acid in the troposphere

depends on the presence of mineral aerosol, as well as on aerosol produced by biomass burning, because the aerosol serves a chemical sink for HNO_3 . The removal of HNO_3 from the atmosphere can also be caused by the sea-salt aerosol, the interaction with which lead to formation of the coarse nitrate aerosol. The formation of nitrate aerosol can also be connected with nocturnal heterogeneous reactions with the participation of NO_3 and N_2O_5 on the moistened surface of sulfate aerosol particles. Both natural and anthropogenic aerosol undergoes the long-range transport, due to which, in particular, the sulfate and nitrate aerosols were detected in remote regions of the Pacific Ocean and the presence of aerosol particles consisting of sulfates, nitrates, organic compounds, black carbon, ashes, and other components was observed over the tropical Indian Ocean.

Ma et al.²¹ discussed the measurement results on the size-resolved ionic aerosols (NH_4^+ , Na^- , K^+ , Ca^{2+} , Mg^{2+} , SO_4^{2-} , Cl^- , NO_3^- , CO_3^{2-} , formate, acetate, and oxalate), organic aerosols, black carbon, and gaseous HNO_3 and SO_2 at the Waliguan Observatory (WO) in the northeastern part of the Tibetan Plateau ($36^\circ 17' \text{N}$, $100^\circ 54' \text{E}$, 3816 m above the sea level) in October–November 1997 and January 1998. The observational data were analyzed with a focus on the partitioning of nitrate between the gas and particle phases. Nitrate was found to exist mainly in the particle phase with a typical particulate-to-total nitrate ratio, i.e., $(\text{NO}_3^-(\text{p})) / (\text{HNO}_3^-(\text{p}) + \text{HNO}_3(\text{g}))$, of about 0.9. It was also found that the size distribution pattern of particulate nitrate at WO varied in different samples and the amount of particulate nitrate residing in the fine mode ($d_p < 2.0 \mu\text{m}$) was typically larger than or comparable with that in the coarse mode.

A gas–particle chemical equilibrium model was used to predict these particulate nitrate size distributions. The size distributions of particulate nitrate were reasonably reproduced with the model within the uncertainties caused by the detection limits. The chemical pathways for the formation of particulate nitrate at WO were analyzed with the size distributions of measured ionic aerosols. It was demonstrated that fine nitrate particles might have been produced by the reaction of gaseous nitric acid with gaseous ammonia, while coarse nitrate particles may have been generated via the condensation of nitric acid on the surface of mineral aerosols. The signature of biomass burning at WO was found to be associated with black carbon as well as the accumulation of potassium and oxalate in the fine particles.

2. Photochemical processes with participation of aerosol

Martin et al.²³ investigated the sensitivity of tropospheric OH, O_3 , and O_3 precursors to

photochemical effects of aerosols not usually included in global models: (1) aerosol scattering and absorption of ultraviolet radiation and (2) reactive uptake of HO_2 , NO_2 , and NO_3 . The sensitivity was calculated by coupling a global 3D model of tropospheric chemistry (GEOS-CHEM) with 3D global fields of sulfate, black and organic carbon, sea-salt and dust aerosols from a global 3D aerosol model GOCART with the same global fields of meteorological parameters. Only the contribution of N_2O_5 hydrolysis in aerosol particles, whose significance was studied earlier and taken into account in modern models of tropospheric chemical processes, was ignored.

The significant aerosol impact manifests itself in a decrease of the photolysis frequency and weaker chemical uptake of HO_2 . The changes in the photolysis frequency are mostly attributed to the effects due to the absorbing aerosol (the influence of the scattering sulfate aerosol is insignificant). In particular, aerosol decreases the photolysis frequency $J(\text{O}(^1\text{D}))$ in the case of transformation $\text{O}_3 \rightarrow \text{O}(^1\text{D})$ near the surface by 5–20% throughout the Northern Hemisphere (largely due to mineral dust) and by a factor of 2 in biomass burning regions (largely due to black carbon). Aerosol uptake of HO_2 accounts for more than 10% of the total HO_x radical (= OH + peroxy) loss in the boundary layer over continental regions.

The effect of heterogeneous chemical reactions on the surface of aerosol particles is the strongest in the regions with the high concentration of fine aerosol, capable of stimulating gas-phase gas-to-particle transformations. In the polluted atmosphere of Eastern Europe (mostly due to sulfate and organic carbon), the aerosol uptake of HO_x achieves 50–70% of the total HO_x loss and exceeds 70% in tropical biomass burning regions (as regards organic carbon). Aerosols cause the decrease in the OH concentration by 5–35% at the most part of the Northern Hemisphere, up to two times in Northern Europe (in August), and up to four times in India (in March). The chemical uptake of NO_2 and NO_3 is relatively weak. Such processes change the NHO_3 concentration by more than 10% only in the tropical Northern Atlantic, in Sahara, and over oceans of the Southern Hemisphere.

In the continental regions, only a slight aerosol-induced increase in the NO_x concentration due to the decrease in the OH concentration is observed. The annual mean globally mean decrease in the OH concentration due to aerosol is 9% (it is comparable with the contribution of hydrolysis caused by N_2O_5), while in the Northern Hemisphere it is 13%. About 60% of the global decrease in the OH concentration is due to the radiative effects of the dust aerosol. The annual mean globally mean level of O_3 production decreases by 6%, but the O_3 budget in the troposphere remains almost unchanged. The CO concentration increases by 5–15 ppbv in the most part of the Northern Hemisphere. Boundary-layer O_3

decreases by 15–45 ppbv over southern Asia during the biomass burning season in March and by 5–9 ppbv over northern Europe in August, and only by 1–3 ppbv in the USA. It can be believed that the surface concentration of ozone in Western Europe and in other industrial regions increases, if atmospheric emissions of aerosol decrease without the accompanying decrease in the concentration of the ozone precursors. The global budget of tropospheric ozone is characterized by the levels of chemical formation (4924 gO₃/year) and loss (4377 gO₃/year).

Ma with co-workers²² investigated the plume of polluted air mass from China over the western Pacific Ocean between 24 February and 10 April 2001. The analysis was based on airborne measurements made during the NASA Transport and Chemical Evolution over the Pacific (TRACE-P) experiment. Fine-particle water-soluble potassium (K⁺) was confirmed to be a unique biosmoke (biomass burning product) tracer. According to data of DC-8 and P-3B flying laboratories, starting from airports in Hong Kong and China and from the USA air force base in Yokota (Japan), the presence of K⁺ in the fine aerosol was observed in about 20% of all cases. It was found that K⁺ correlated with absorbing aerosol particles ($r^2 = 0.73$), ammonium ($r^2 = 0.77$), and CO ($r^2 = 0.61$). In the observations considered, the correlation between the concentrations of K⁺ and CO turned out to be higher than that between methyl chloride (CH₃Cl) and CO ($r^2 = 0.50$), which is often used as a biosmoke tracer. The absence of correlation between K⁺ and sodium or calcium indicates that the contributions of sea-salt aerosol and mineral dust to formation of the K⁺ concentration were insignificant.

Most biomass burning plumes were found in the latitude belt of 15–25°N at the altitudes of 2–4 km. The air mass back trajectories of these plumes generally originated from the southeast Asia. In these cases, the increased concentration of K⁺, NH₄⁺, NO₃⁻, and the absorbing aerosol particles (with the mutual correlation) was observed. In the atmospheric boundary layer at latitudes above 25°N, highly mixed urban/industrial and biosmoke plumes, indicated by SO₄²⁻ and K⁺, were observed in 5 out of 53 plumes located to the north from 25°N. Similar situation was also observed 1 month later during ACE-Asia. The air mass back trajectories of these mixed plumes generally passed through the latitude range between 34° and 40°N of the eastern China coast, a region that includes the large urban centers of Beijing and Tianjin.

Sources of biosmoke in these cases were likely biomass burning sites. To characterize the relative contribution of biosmoke to formation of mixed plumes, the data on the molar ratios dK^+/dSO_4^{2-} and SO₂/CO were used for the fine aerosol. According to the data on dK^+/dSO_4^{2-} , correlation can be found between the relative contribution of biosmoke and the

concentration of inorganic fine aerosol ($r^2 = 0.93$), as well as the volume of the fine aerosol fraction ($r^2 = 0.85$). The mixed plume with the maximum values of the volume (mass) of the fine aerosol, K⁺, NH₄⁺, NO₃⁻, SO₄²⁻, the absorbing (soot) aerosol, and CO was found in the Yellow Sea. Biosmoke made up about 60% of this plume. On the average, the biosmoke contribution was about 35–40% with respect to the mass of the inorganic fine aerosol in mixed plumes observed to the north from 25°N.

In recent years, numerous investigations of the effect of tropospheric aerosol on chemical reactions (budget of various trace gases) and photolysis processes have been carried out at individual sites and on the regional scales. However, no attempts have been made to generalize the results obtained on the global scale and for long periods (about decades), which is necessary for estimation of the global budgets of trace gases and their contributions to formation of the greenhouse effect. This situation is partly caused by the lack of the needed reliable information about the aerosol properties, formalized in the form of global aerosol models. The main source of such information is, certainly, only the spaceborne remote sensing of aerosol.

Bian et al.² analyzed the aerosol impact on global budgets of O₃, OH, and CH₄ through the aerosol-induced changes in the photolysis rate and the direct effect of heterogeneous chemical reactions on the surface of aerosol particles. The first effect was evaluated with a global tropospheric chemistry transport model using recently developed global models of tropospheric aerosols: a satellite-derived aerosol model over the oceans and a model for land plus oceans. Globally averaged, the impact of aerosols on photolysis alone is to increase tropospheric O₃ by 0.63 Dobson units and increase tropospheric CH₄ by 130 ppb (via the decrease of the tropospheric OH by 8%). The increase of these greenhouse gases leads to an indirect radiative forcing (with the count of both natural and anthropogenic aerosols) of +0.08 W/m².

Although the CH₄ increase is, of course, global, the changes in tropospheric OH and O₃ are mainly regional, with the largest impacts in the northwest Africa in January and in India and southern Africa in July. The influence of aerosols is greater in July than in January and greater in the Northern Hemisphere than in the Southern Hemisphere. The predominant impact is due to the aerosols over land; aerosols over the ocean contribute less than a third to globally integrated changes.

Lefer et al.¹⁹ compared the photolysis frequency measurements by the NCAR scanning actinic flux spectroradiometer (SAFS) and the calculations from a cloud-free model (CFM). Overall, the mean measured-to-model ratio of jNO_2 for all flights of TRACE-P was 0.943 ± 0.271 . The sky conditions during the Transport and Chemical Evolution over the Pacific (TRACE-P) experiment were determined

to be "cloud-free" 40% of the time; hence a CFM is frequently not representative of the local atmospheric conditions. The analysis indicated that clouds have a larger impact on photolysis frequencies (from -90 to +200%) than do aerosols (maximum of $\pm 20\%$).

The CFM and SAFS j_{NO_2} and $j(\text{O}^1\text{D})$ values differed by 9% and 0–7%, respectively, during a vertical profile through a cloud-free and low AOD atmosphere. This suggests that measurement/model agreement to less than 10% may be difficult without better aerosol optical parameter inputs even under low-AOD conditions. For the TRACE-P chemical environment, OH, NO, and HO₂ were more sensitive than other compounds (e.g., CH₃C(O)O₂, CH₃OOH) to changes (or errors) in photolysis frequency inputs to a photochemical box model.

Compounds including NO₂, PAN, and HCHO exhibited different relationships to j -value changes below and above the boundary layer. Ozone production and loss rates increased linearly with changes (or errors) in the photolysis frequency with the resulting net O₃ tendency increasing. During the TRACE-P mission the net photochemical effect of clouds and aerosols was a large decrease in photochemical O₃ production in the boundary layer.

The growing level of atmospheric pollution determines the urgency of improvement of air quality models (AQM). In this context, Rodriguez and Dabdub²⁵ analyzed the global data on the sensitivity of AQM to pollutant emissions into the atmosphere using the numerical simulation model, developed at the California Institute of Technology. Emphasis was placed on the characterization of uncertainties for product concentrations that constitute secondary organic aerosol (SOA). The sensitivity analysis of the chemical mechanism determining the SOA concentration was performed using Monte Carlo techniques.

Uncertainties in rate parameters were analyzed for three different summer cases. Cases studied cover a range of initial concentrations of reactive organic gases and nitrogen oxides that represent episodes of high ozone levels in polluted urban areas. In addition to estimated uncertainties of gas-phase SOA precursor concentrations, similar calculations were performed for O₃, HCHO, H₂O₂, and peroxyacetyl nitrate (PAN).

Results indicate that SOA precursor concentrations predicted using nominal CACM rate parameters were similar to estimates by the Monte Carlo simulations. The SOA gas-phase precursors in CACM presented relative errors that range from 30% at a VOC/NO_x ratio of 8:1 to 39% when the ratio changes to 32:1. Although the results discussed have demonstrated that the reactions associated with photooxidation of aromatic compounds and direct transformation of aldehydes into the semivolatile organic acids are not the most significant ones for formation of SOA, the estimated effect of change in the rate parameters of the reactions agrees with the earlier obtained data.

An important new conclusion is that the most significant factors of reliability of the pre-calculated SOA concentration is the reliability of information about photolysis of NO₂ and HCHO, and about the reaction between aromatic compounds and OH at the VOC/NO_x ratio smaller than 17:1. The concentrations of SOA precursors depend most strong on the OH loss in the reaction with NO₂ at low VOC/NO_x. However, if this ratio is high, the reaction of O₃ with NO plays the most significant role in the formation of SOA.

During the Atlanta Supersite Experiment (ASSE) in August 1999, a three-channel particle composition monitor (PCM) was used to measure PM_{2.5} mass and composition as well as gas-phase NH₃, HCl, HNO₃, HONO, SO₂, and acetic, formic, and oxalic acids over integrating periods of 10–24 hours. The period was characterized by stagnation periods associated with high temperatures, high relative humidities, and UV radiation, underlying parameters causing photochemical activity with intense ozone, and PM_{2.5} formation. Analysis of diurnal measurements carried out by Baumann et al.¹ pointed to photochemical sources of HNO₃, HONO, acetic, and formic acids. It is found, however, that the specific features of the measurement technique caused underestimation of [HNO₃] and correspondingly overestimation of [HONO]. Peculiarities of processing the measurement data on the content of organic carbon in aerosol, connected with the empirical correction for other (ignored) organic elements (OOE) (OOE = 0.6 × organic carbon (OC)), were discussed. Despite this correction, the average percent fraction of unidentified mass of 13 ± 10% relative to the total reported mass concentration still remained. However, if additional filter samples were included, an almost complete closure in the mass balance is achieved.

It can be speculated that photochemically well-aged and well-mixed air masses contain organic compounds with higher oxygenated and less volatile functional groups, whereas under more stagnant conditions, particle-phase organics might be less oxygenated and therefore more volatile. Sulfate and all organic compounds (including particle bound light organic acids, organic carbon, and OOE) are the main identified contributors to the overall PM_{2.5} mass with 33 ± 8 and 39 ± 12%, respectively. Acidity calculations based on the particle-phase SO₄²⁻/NO₃⁻/NH₄⁺ system showed slightly acidic conditions.

For a long time (especially, in the context of acid rains), the great attention is paid to the investigations of pH for the aqueous phase in the atmosphere. By now, the mechanisms of formation of acid precipitation have been studied quite adequately. It has been shown in particular, that pH for droplets is one of the most significant parameters, characterizing the dynamics of chemical reactions in the aqueous phase in the atmosphere. In cloud droplets, the rate of oxidation processes depends

strongly on pH, which is mostly caused by the decrease in the solubility of trace gases with the decrease of pH. Changes of pH affect also the solubility of trace metals and, consequently, alternate catalytic cycles with participation of metals in droplets. The pH level of droplets is determined by the balance between the present acid and neutralizing components.

The main acid components of mostly anthropogenic origin are H_2SO_4 and HNO_3 , whose precursors are, respectively, SO_2 and NO_x , whereas the neutralizing components are ammonium NH_4^+ , existing mostly in the gas phase, and mineral aerosol particles. If the process of gas dissolution can be described quite well using the Henry law and the processes of diffusion accommodation, then the process of aerosol dissolution remains unclear in many respects.

Desboeufs with co-workers⁵ discussed the results of laboratory investigations of pH, which allowed them to reconstruct the process of dissolution of aerosol particles in cloud droplets and to analyze in what way these particles can affect the droplet pH. The effect of aerosol of two types, of the soil and anthropogenic origin, was analyzed. The experiments conducted in an open-flow system showed that the pH changes induced by aerosol solubilization last up to 30 min, in the range of a typical droplet lifetime. These pH changes depend on the initial pH of the experiment. In the pH range between 3 and 5, the pH varies most strongly when it is high.

In Ref. 5, a relationship between the neutralizing capacity of the aerosol (NCA), i.e., the amount of uncompensated base species, and the pH after neutralization has been found. The NCA is related to the aerosol composition: silicates present more or less pronounced NCA, whereas C graphite presents a negative NCA, i.e., an acidifying capacity. The aerosol composition can be modified during cloud evaporation and condensation, notably by the addition of sulfate or sulfuric acid to the aerosol surface. NCA modification with cloud processing is observed when the amount of dissolved acid is larger than the neutralizing capacity of the aerosol.

The results of laboratory experiments carried out by Kalberer with co-workers¹³ have demonstrated that the photooxidation of organic compounds results in formation of a significant fraction of aerosol consisting of polymers, and the polymerization proceeds due to the reactions between carbonyls and their hydrates. Upon the analysis of natural organic compounds emitted into the atmosphere by Amazonian tropical rain forests, Claeys et al.⁴ detected a considerable amount of polar organic compounds (polyols), which have not been observed earlier. The low vapor pressure of such polyols favors their condensation on aerosol particles. The estimates showed that, on the global scale, isoprene photooxidation may produce about 2 Tg polyols, which comprises a significant fraction of the total biogenic production of secondary aerosol (8–40 Tg).

The problem of formation of the secondary aerosol due to gas-phase oxidation of organic compounds was discussed in detail by Griffin et al.^{7,8} Laskin et al.¹⁷ carried out a laboratory investigation of the reactions on the surface of aerosol particles, which serve a source of sulfates in the sea-salt aerosol particles.

Conclusions

The obvious conclusion from the brief review presented above is that the investigations into the interaction of aerosol and atmospheric trace gases are still at the initial stage.

References

1. K. Baumann, F. Ilt, J.Z. Zhao, and W.L. Chameides, *J. Geophys. Res. D* **108**, No. 7, SOS 4/1–SOS 4/20 (2003).
2. H. Bian, M.J. Prather, and T. Takemura, *J. Geophys. Res. D* **108**, No. 8, ACH 4/1–ACH 4/10 (2003).
3. H. Bian and C.S. Zender, *J. Geophys. Res. D* **108**, No. 21, ACH 8/1–ACH 8/14 (2003).
4. M. Claeys, B. Graham, G. Vas, W. Wang, R. Vermeylen, V. Pashynska, J. Cafmeyer, P. Guyon, M.O. Andreae, P. Artaxo, and W. Maenhaut, *Science* **303**, No. 5661, 1173–1176 (2004).
5. K.V. Desboeufs, R. Losno, and J.L. Colin, *J. Atmos. Chem.* **46**, No. 2, 159–172 (2003).
6. A. Gelenczér, A. Hoffer, Z. Krivácsy, G. Kiss, A. Molnár, and E. Mészáros, *J. Geophys. Res. D* **107**, No. 21, ICC 2/1–ICC 2/6 (2002).
7. R.J. Griffin, D. Dabdub, and J.H. Seinfeld, *J. Geophys. Res. D* **107**, No. 17, AAC 3/1–AAC 3/26 (2002).
8. R.J. Griffin, K. Nguyen, D. Dabdub, and J.H. Seinfeld, *J. Chem.* **44**, 171–190 (2003).
9. R.G. Hynes, M.Z. Fernandez, and R.A. Cox, *J. Geophys. Res. D* **107**, No. 24, AAC 18/1–AAC 18/11 (2002).
10. M.Z. Jacobson, *J. Geophys. Res. D* **107**, No. 19, AAC 2/1–AAC 2/23 (2002).
11. C.E. Jordan, J.E. Dibb, B.E. Anderson, and H.E. Fuelberg, *J. Geophys. Res. D* **108**, No. 21, GTE 38/1–GTE 38/10 (2003).
12. B. Jourdain and M. Legrand, *J. Geophys. Res. D* **107**, No. 22, ACH 20/1–ACH 20/13 (2002).
13. M. Kalberer, D. Paulsen, M. Sax, M. Steinbacher, J. Dommen, A.S.H. Prevot, R. Fisseha, E. Weingartner, V. Frankevich, R. Zenobi, and U. Baltenspreger, *Science* **303**, No. 5664, 1659–1662 (2004).
14. K. Kawamura, N. Umemoto, and M. Mochida, *J. Geophys. Res. D* **108**, No. 23, ACE 7/1–ACE 7/7 (2003).
15. S. Korontzi, D.E. Ward, R.A. Susott, R.J. Yokelson, C.O. Justice, P.V. Hobbs, E.A.H. Smithwick, and W.M. Hao, *J. Geophys. Res. D* **108**, No. 24, ACH 7/1–ACH 7/14 (2003).
16. B.J. Krueger, V.H. Grassian, A. Laskin, and J.P. Cowin, *Geophys. Res. Lett.* **30**, No. 8, 48/1–48/4 (2003).
17. A. Laskin, D.J. Gasper, W. Wang, S.W. Hunt, J.P. Cowin, S.D. Colson, and B.J. Finlayson-Pitts, *Science* **301**, 340–344 (2003).
18. Y.-N. Lee, R. Weber, Y. Ma, D. Orsini, K. Maxwell-Meier, D. Blake, S. Meinardi, G. Sachse, C. Harward, T.-Y. Chen, D. Thornton, F.-H. Tu, and A. Bandy, *J. Geophys. Res. D* **108**, No. 23, ACE 14/1–ACE 14/14 (2003).

19. B.L. Lefer, R.E. Shetter, S.R. Hall, J.H. Crawford, and J.R. Olson, *J. Geophys. Res. D* **108**, No. 21, GTE 42/1–GTE 42/12 (2003).
- 19a. H. Liao, P.J. Adams, S.H. Chung, J.H. Seinfeld, L.J. Mickley, and D.J. Jacob, *J. Geophys. Res. D* **108**, No. 1, 1/1–1/23 (2003).
20. W. Liu, P.K. Hopke, and R.A. Van Curen, *J. Geophys. Res. D* **108**, No. 23, AAC 1/1 – AAC 1/18 (2003).
21. J. Ma, J. Tang, S.-M. Li, and M.Z. Jacobson, *J. Geophys. Res. D* **108**, No. 17, ACH 8/1–ACH 8/12 (2003).
22. Y. Ma, R.J. Weber, Y.-N. Lee, D.A. Orsini, K. Maxwell-Meier, D.C. Thornton, A.R. Bandy, D.R. Clarke, G.W. Sachse, H.E. Fuelberg, C.M. Kiley, J.-H. Woo, D.G. Streets, and G.R. Carmichael, *J. Geophys. Res. D* **108**, No. 21, GTE 37/1–GTE 37/16 (2003).
23. R.V. Martin, D.J. Jacob, R.M. Yantosca, M. Chin, and P. Ginoux, *J. Geophys. Res. D* **108**, No. 3, ACH 6/1–ACH 6/14 (2003).
24. A. Meier and J. Hendricks, *J. Geophys. Res. D* **108**, No. 23, ACH 9/1–ACH 9/16 (2003).
25. M.A. Rodriguez and D. Dabdub, *J. Geophys. Res. D* **108**, No. 15, 2/1–2/9 (2003).
26. I. Tegen, S.P. Harrison, K. Kohfeld, I.C. Prentice, M. Coe, and M. Heimann, *J. Geophys. Res. D* **107**, No. 21, AAC 14/1–AAC 14/27 (2002).
27. D. Trochikine, Y. Iwasaka, A. Matsuki, M. Yamada, Y.-S. Kim, T. Nagatani, D. Zhang, G.-Y. Shi, and Z. Shen, *J. Geophys. Res. D* **108**, No. 23, ACE 10/1–ACE 10/11 (2003).
28. S. Wang, R. Ackermann, C.W. Spicer, J.D. Fast, M. Schmeling, and J. Stitz, *Geophys. Res. Lett.* **30**, No. 11, 49/1–49/4 (2003).